



Article

Evaluation of Hybrid Fiber Multiscale Polymer Composites for Structural Confinement under Cyclic Axial Compressive Loading

Lakshmi Joseph ¹, Mini K. Madhavan ^{1,*}, Karingamanna Jayanarayanan ^{2,3,*}  and Alessandro Pegoretti ⁴ 

¹ Department of Civil Engineering, Amrita School of Engineering, Amrita Vishwa Vidyapeetham, Coimbatore 641112, India; j_lakshmielizabeth@cb.students.amrita.edu

² Department of Chemical Engineering and Materials Science, Amrita School of Engineering, Amrita Vishwa Vidyapeetham, Coimbatore 641112, India

³ Center of Excellence in Advanced Materials and Green Technologies (CoE-AMGT), Amrita School of Engineering, Amrita Vishwa Vidyapeetham, Coimbatore 641112, India

⁴ Department of Industrial Engineering, University of Trento, 38123 Trento, Italy; alessandro.pegoretti@unitn.it

* Correspondence: k_mini@cb.amrita.edu (M.K.M.); kj_narayanan@cb.amrita.edu (K.J.)

Abstract: Fiber reinforced polymer (FRP) confinement is recognized as the most promising technique for the strengthening and retrofitting of concrete structures. In order to enhance the performance of conventional epoxy-based FRP composites, nano filler modification of the epoxy matrix was implemented in the current study. In particular, the cyclic loading response of standard concrete specimens externally confined by epoxy-based natural and hybrid fiber reinforced polymer systems was investigated. The confinements were realized with sisal fiber reinforced polymer (SFRP) and hybrid sisal basalt fiber reinforced polymer (HSBFRP). Moreover, the effects of multiwalled carbon nanotubes (MWCNT) were also investigated. Three different specimen sets were considered for study: (i) unconfined specimens, (ii) epoxy-based FRP confined specimens and (iii) MWCNT incorporated epoxy-based FRP confined specimens. The specimens were tested in repeated compressive mode in loading-unloading cycles at increasing displacement levels. The test results revealed that FRP wrapping could enhance the mechanical behavior of unconfined columns in terms of strength and ductility. Moreover, it was evident that the mechanical properties of the epoxy matrix were enhanced by MWCNT incorporation. The developed epoxy-based FRP confinement containing MWCNT ensures improvement in axial strength by 71% when compared with unconfined specimens. The epoxy-based FRP confinement, with and without MWCNT, exhibited a high strain redistribution behavior around the concrete core. In comparison to the unconfined specimens, the confinement could increase the sustained axial strain from 0.6 to 1.4% using epoxy-based FRP confinement and to 1.6% with MWCNT incorporated epoxy-based FRP confinement. Further, an empirical model was developed to predict the ultimate axial stress of concrete columns confined externally with FRP jackets. The ultimate compressive strength obtained from the experimental study was compared with the proposed model, and the observed deviation was lower than 1%.

Keywords: epoxy; MWCNT; sisal fiber; basalt fiber; multiscale composites; confinement; retrofitting; cyclic axial compression



Citation: Joseph, L.; Madhavan, M.K.; Jayanarayanan, K.; Pegoretti, A. Evaluation of Hybrid Fiber Multiscale Polymer Composites for Structural Confinement under Cyclic Axial Compressive Loading. *J. Compos. Sci.* **2023**, *7*, 152. <https://doi.org/10.3390/jcs7040152>

Academic Editor: Francesco Tornabene

Received: 1 March 2023

Revised: 13 March 2023

Accepted: 3 April 2023

Published: 9 April 2023



Copyright: © 2023 by the authors. Licensee MDPI, Basel, Switzerland. This article is an open access article distributed under the terms and conditions of the Creative Commons Attribution (CC BY) license (<https://creativecommons.org/licenses/by/4.0/>).

1. Introduction

The deterioration in concrete structures may have different causes, such as errors occurring during design and construction stages, fatigue failure, and exposure to harsh environments which induces severe structural damage. Hence, to maintain structural integrity, there is a pressing need for the development of various retrofitting techniques which could ensure structural safety along with extended serviceability. In reinforced concrete (RC) structures, external strengthening through the FRP system is a preferred option with regard to the conventional strengthening systems based on steel and concrete jacketing [1,2]. External confinement with –FRP systems results in considerable enhancement in stress

and strain responses, thereby upgrading the ultimate load carrying capacity [3–5]. An improved stress–strain response of concrete columns is reported, corresponding to different external FRP confinements under monotonic or cyclic axial compression [6–8].

Carbon, glass, aramid, etc. are the fibers conventionally used in FRP composites [9–11]. High strength and modulus are the attributes for their selection in FRP systems. The glass fiber reinforced polymer (GFRP) confinements were effective in enhancing the ductility and strength of the concrete core [12,13]. However, recently, an emerging trend has been the usage of natural fibers in FRP composites as a replacement for conventional synthetic fibers. In fact, natural fibers such as sisal, jute, abaca, and flax fiber, which have moderate tensile and flexural properties, when used in fiber reinforced polymers were effective in retrofitting concrete columns [14–16]. The usage of natural fibers in strengthening application is considered to be a renewable and sustainable solution. In India, a wide range of natural fibers, such as jute, sisal, banana, etc. are abundantly available. The sisal and jute confinements are effective in enhancing the load carrying and energy absorbing characteristics. Further investigations revealed that hybridization of natural and synthetic FRP systems facilitated an excellent option for structural retrofitting. Hybrid composites like Jute–polyester [17], Sisal–GFRP [18], and Abaca–Jute–GFRP [19] have exhibited superior performance over the individual natural FRP systems [20]. They reported increments in strain and energy dissipation characteristics corresponding to hybrid configurations.

Bouchelaghem et al. [21] conducted a study comparing the conventional CFRP systems and newly developed hybrid FRP systems, and reported that hybrid confinement was effective in offering a cost-effective solution. The behaviors of stress–strain plots and post-peak load regimes were analyzed by De Luca et al. [22], and they noticed minor load drops during the strain increments. Furthermore, they reported that the ductility and energy dissipation characteristics could be improved by hybrid FRP confinement. Takeuti et al. [23] carried out the investigation on differently-shaped concrete columns which were strengthened with the FRP system. The specimens were preloaded and then were subjected to axial compression loads. It was seen that even though preloading results in poor ductility, there was no significant impact on the load-carrying capacity. Observations were also made that circular columns exhibited better ductility characteristics than square columns. Rousakis et al. [24] analyzed the performance of FRP-confined RC square sections under repeated load-unload axial compressive cycles and found that upon FRP confinement a remarkable upgradation in both strength and strain ductility was noticed. In a recent study [25], the effect of predamage and loading cycles on the confined concrete was analyzed [25]. The test results revealed that concrete predamage has a substantial effect on the cyclic stress–strain curve of the FRP-confined concrete under cyclic loading.

The widely used matrix material in FRP composites is the thermoset polymer epoxy resin. High strength and stiffness along with chemical compatibility make it a correct option as the matrix material [26]. During the service period, epoxy composites are exposed to severe environmental conditions which result in the degradation of epoxy resin and its various mechanical characteristics [27]. The behavior of FRP laminates depends on the choice of components, volume fraction, and the manufacturing process [28–30]. The multi-scale composites have grabbed the attention of researchers worldwide [31], as they are composites with macro fibers along with nanoscale materials used as matrix reinforcement. The unique properties of carbon nanotubes (CNTs) compared to other reinforcements make it a good option to be used as nanofillers in the polymer matrix. CNTs are classified into single-walled carbon nanotubes (SWCNT) and multiwalled carbon nanotubes (MWCNT) [32]. They possess good resilience, which can sustain large angle bending without damage [33]. When CNTs were incorporated into the traditional polymer composite, it was found to significantly enhance their various mechanical and durability properties [34]. The higher surface area offered by these nanoparticles ensures a better filler–polymer interface interaction and improved stress transfer within the matrix. However, at higher concentrations of nanoparticles, there were agglomerations of CNTs which was due to the Van der Waals forces between the individual nanotubes [35]. Hence, uniform dispersion of CNTs in epoxy

resin is carried out either by sonication or high shear mixing. Eskizeybek et al. [36] studied the performance of epoxy/carbon fiber composites. The overall load-carrying capacity was upgraded noticeably, resulting in improvement in general material toughness. Kumar P.S. et al. [37,38] stated that upon MWCNT incorporation in epoxy a considerable enhancement in tensile and fracture properties of the composites was observed. The carbon fiber acts as a macroscale reinforcement, whereas MWCNT assumes the role of a nanofiller in the epoxy matrix, resulting in a multiscale composite. They inferred that MWCNT addition beyond the optimum content led to a reduction in properties due to clustering of MWCNTs. Joseph et al. [39] explored the performance of nano filler modified epoxy-based FRP confinement under monolithic axial compression and found that the newly developed FRP confinement could improve the strength properties considerably. The high temperature performance of these confinements was also found to be superior [40].

As evident from the literature, the in-depth analysis of hybrid sisal basalt fiber-reinforced polymer (HSBFRP) is not fully explored. The efficiency of MWCNT dispersed in epoxy-based hybrid sisal-basalt FRP as a confinement system in concrete columns under repeated axial compression, decompression, and recompression cycles is critically investigated in this work. The cost involved in MWCNT could be justified by strength enhancement, and the studied hybrid system can be used as an alternative to the conventional high-cost CFRP system. The peak strength obtained for different confinement systems from the experimental study is compared with various existing models. To evaluate the peak compressive strength of the newly developed hybrid sisal basalt epoxy-based FRP system, a modified mathematical model is derived from previous reports [41,42]. This study is focused to explore the feasibility of the newly developed FRP system as a strengthening material for structural applications.

2. Experimental Work

For the axial cyclic compressive loading test, concrete specimens of dimensions height 300 mm and diameter 150 mm were used. This experimental program consists of a series of studies relating to unconfined columns and influence of external FRP confinement. Four different types of confinements were considered in the study: (i) epoxy-based sisal fiber reinforced polymer (SFRP) sheets; (ii) epoxy-based SFRP sheets with incorporated MWCNT; (iii) epoxy-based hybrid SBFRP sheets; (iv) epoxy-based hybrid SBFRP sheets with incorporated MWCNT.

2.1. Materials Used

2.1.1. Concrete

Grade 53 Ordinary Portland Cement meeting the requirements of IS 12269-2013 was used for the preparation of concrete. Concrete mix proportioning was carried out for a characteristic compressive strength of 20 MPa as per IS 10262-2019. The mix ratio was calculated as 1:1.5:2.58 as weight of cement: FA: CA with a water cement ratio of 0.45. The concrete cylinders were cast, and water cured for a period of 28 days. The material properties are described in Table 1.

Table 1. Constituent properties of materials.

Material	Property	Value
Cement	Grade	53
	Specific Gravity	3.15
Fine aggregate	Fineness modulus	2.83
	Specific Gravity	2.63
Coarse aggregate	Bulk density	1.52 kg/L
	Specific gravity	2.64

Table 1. *Cont.*

Material	Property	Value
MWCNT	nanotube purity	97%
	average length	2–10 microns
	specific surface area	250–270 m ² /g
Sisal fiber	Thickness	0.8–1.1 mm
	GSM	300
	Density	1582 kg/m ³
Basalt fiber	Thickness	0.8–1.1 mm
	GSM	380
	Density	2633 kg/m ³

2.1.2. MWCNT Modified Epoxy Resin

Two-part high-performance epoxy resin was used as the matrix consisting of resin and hardener blended in a mix ratio of 100:15 as suggested by the supplier (Covai Seenu, Coimbatore, India). To improve the adhesion properties of epoxy and, thereby, to enhance the strength, MWCNT modified with carboxylic acid (–COOH) was chosen as the nano filler, which was supplied by Platonic Nanotech Private Ltd., Mahagama, India.

2.1.3. Fiber

Bidirectional woven plain sisal and basalt fibers with identical thickness were used as the fiber reinforcement in the FRP composites. Basalt fiber and sisal fibers were supplied by Go Green Products, India. Being a natural fiber, alkali treatment was carried out on sisal fibers prior to wrapping. These fibers were completely immersed in alkaline solution (NaOH), after which they were dried in a controlled environment for 72 h [43].

2.2. FRP Composite Preparation

The composite laminates were prepared by a two-step hand layup method. In the first step, within the epoxy resin the MWCNT was homogeneously distributed for 30 min using an ultrasonic probe sonicator of 20 kHz capacity. Subsequently, the hardener was mixed with the epoxy matrix in a ratio of 100 parts by weight of resin to 15 parts by weight of hardener. The second stage included the laminate preparation with various fibers systems embedded in the epoxy resin containing 1 wt.% of MWCNT [44]. The laminates were then cured for 72 h at room temperature. The cured laminates were then cut into specific dimensions: 100 mm length, 10 mm width and 3 mm thickness based on the test requirements as per ASTM D3039, as seen in Figure 1.

2.3. Preparation of Confined Specimen

Five different sets of specimens were considered and prepared for the study as unconfined specimens, SFRP confined specimens, HSBFRP confined specimens, MWCNT modified epoxy-based SFRP confined specimens, and MWCNT modified epoxy-based HSBFRP confined specimens. Concrete cylindrical specimens of the dimensions 300 mm in height and 150 mm in diameter were cast and water-cured for a standard period of 28 days. After curing, the specimens were dried, and the concrete surfaces were then cleaned and roughened for FRP wrapping. MWCNTs were carefully mixed with the epoxy resin until a homogeneous mixture was obtained. Over the roughened surface of concrete, a layer of prepared epoxy resin was applied using a roller. When hybrid confinement was taken into consideration, sisal fiber sheets impregnated with epoxy were wrapped around the concrete cylinder as the inner layers, and on top of them basalt fiber layers were wrapped around. In between every layer, the epoxy resin was applied as a matrix. An overlap distance of 150 mm was provided for every FRP layer to avoid slippage during

loading. The FRP-confined specimens were then cured in a controlled environment prior to testing. An illustration of FRP-confined specimen preparation is provided in Figure 2. The nomenclature and details adopted for each specimen is given in Table 2. Group A are the laminate specimens used for assessing the properties of MWCNT modified epoxy-based composites, whereas group B represents the concrete column specimens considered for assessing the effect of FRP confinement.

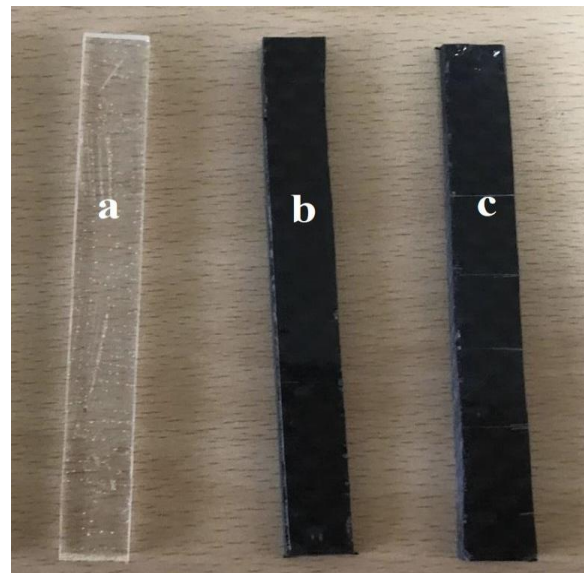


Figure 1. Laminate samples for testing (a) E (b) E-C1 (c) E-C1S2B2.

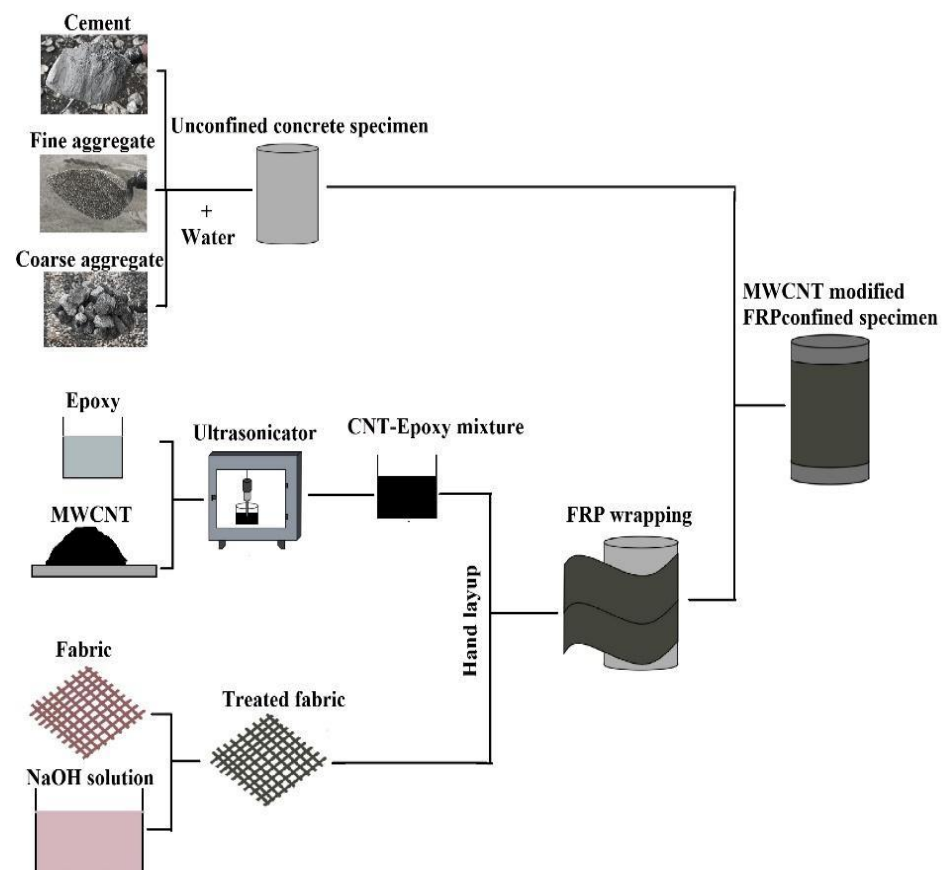


Figure 2. Schematic representation of the preparation of FRP confined specimens.

Table 2. Specimen details and nomenclature.

Group	Specimen Nomenclature	Specimen Material	MWCNT wt.% in FRP	Sisal Layer Count	Basalt Layer Count	Total No. of Fiber Layers
A	E	Epoxy	0	0	0	0
	E-C1	Epoxy	1	0	0	0
	E-C0S2	Epoxy	0	2	0	2
	E-C1S2	Epoxy	1	2	0	2
	E-C0S2B2	Epoxy	0	2	2	4
	E-C1S2B2	Epoxy	1	2	2	4
B	CS	Concrete	0	0	0	0
	C-C0S2	Concrete	0	2	0	2
	C-C1S2	Concrete	1	2	0	2
	C-C0S2B2	Concrete	0	2	2	4
	C-C1S2B2	Concrete	1	2	2	4

2.4. Characterization Techniques

During the first phase of the experimental study, various mechanical properties of epoxy composites were analyzed (specimen details are represented as Group A in Table 2). To analyze the dispersion and morphology of MWCNT in the epoxy matrix, high-resolution transmission electron microscopy (HRTEM) observations were carried out on ultrathin sections of nano composites in a JEOL/JEM 2100 transmission electron microscope at 200 kV acceleration voltage. The tensile properties of the composites were evaluated according to ASTM D3039 in INSTRON 4502 universal testing machine at a cross head speed of 1 mm/min. The dimensions of the epoxy specimens were fixed as 100 mm, 10 mm, and 3 mm, respectively, as length, width, and thickness of the specimen. The flexural strength of the composite was determined as per ASTM D790 at a crosshead speed of 1.25 mm/min by 3-point bending mode test. A single-edge notch bending (SENB) test was conducted as per ASTM D5045 at a load of 20 kN at a cross head speed of 1 mm/min to estimate the fracture toughness.

In the second phase of the study, the influence of FRP jacketing on short concrete columns was studied (specimen details are given in Group B of Table 2). The concrete columns were tested in a universal testing machine (UTM) with a load capacity of 3000 kN until failure under axial compression. The test consisted of repeated axial compression followed by decompression followed by recompression cycles under incremental axial deformations per cycle. The axial deformation was incremented by 1% strain after each cycle. To ensure uniform loading over the concrete specimens, 5mm thick steel plates were placed at both the ends of specimens during testing.

3. Results and Discussion

3.1. Group A Specimens

3.1.1. High-Resolution Transmission Electron Microscopy (HRTEM) of Epoxy Nanocomposites

MWCNTs were added as 0.5, 1.0, 1.5 weight percentages in the epoxy matrix and the morphology, particle size, and alignment of the filler system in the epoxy matrix was examined. The TEM images corresponding to epoxy-MWCNT composites such as EC0.5, EC1, and EC1.5 are shown in Figure 3. The transmission electron microscopy reveals the nanoscale dispersion of MWCNTs in the epoxy matrix. Figure 3b (EC1 composites) reveals that 1 wt.% MWCNT is well dispersed in the epoxy matrix, and even after ultrasonication, MWCNT particles could retain their tubular shape. The multifarious entanglement of epoxy together with MWCNTs leads to better stress transfer, which may further prevent crack propagation within the composites [45]. While EC1.5 (Figure 3c) composites were

considered, i.e., at higher weight percentages of MWCNTs nano filler particle clusters than could be observed, which were still not separated even after the process of ultrasonication. The morphology shows a blend of MWCNT dispersion in certain regions along with agglomeration at a few locations. The formation of clusters could reduce the interfacial area between the epoxy and MWCNT, which may further reduce physical and chemical bonding between them [46]. The major factor which governs the formation of clusters is the interparticle van der Waals force within the MWCNTs [47]. The interparticle distance reduces at the higher nano filler content, which results in the agglomeration of MWCNTs. For the aforementioned reasons, a content of 1 wt.% of MWCNT in epoxy is considered to be an optimal amount for the further study.

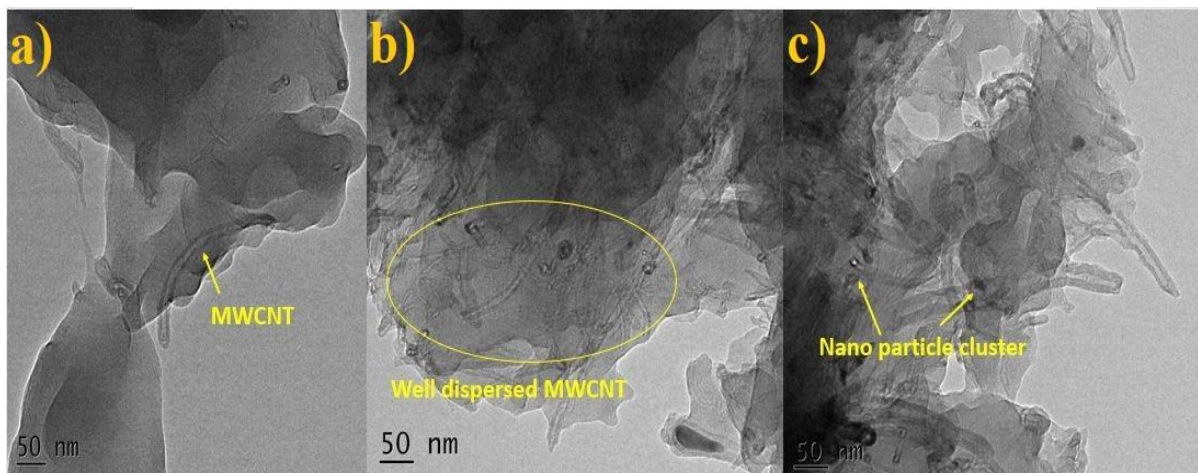


Figure 3. TEM images corresponding to (a) E-C0.5 (b) E-C1 (c) E-C1.5.

3.1.2. Mechanical Properties of Epoxy Nano and Hybrid Composites Tensile Properties

The incorporation of MWCNT in epoxy considerably improved its tensile properties as observable from Table 3. In fact, after dispersion of 1wt.% of MWCNT, enhancements in tensile strength and Young's modulus by 65% and 41%, respectively, compared to the neat epoxy specimens were observed. The rise in tensile strength is due to the uniform dispersion of MWCNT within the epoxy resin, which further provides greater interfacial area and interaction, thus creating an anchoring effect between the epoxy resin and the MWCNTs [48]. Composites with four layers of hybrid sisal and basalt fibers (E-C0S2B2) exhibited an improvement in tensile strength by 94%, and upon addition of 1 wt.% MWCNT to the same hybrid system (E-C1S2B2), the tensile strength was enhanced by 167%. During the loading process, the presence of MWCNT is expected to improve the load-bearing capacity of the FRP confinement [49]. Within the composite, being a low modulus component, the crack initiation begins first at the epoxy during the loading process. The presence of MWCNTs enables a bridging effect within the epoxy matrix, thus increasing its crack propagation resistance [37]. When multiscale composites are considered (E-C1S2B2), a more ductile mode of failure can be observed when compared to neat epoxy composites, due to an increase in the elongation at the break with the MWCNT addition.

Fracture Toughness

The fracture toughness under the opening mode (mode I) was evaluated both as the critical value of the stress intensity factor (K_{IC}) and as the critical value of the strain energy release rate (G_{IC}) [50]. The epoxy when reinforced with sisal and basalt fibers recorded a rapid increase in fracture toughness as given in Table 4. The resistance against delamination growth was provided by the fiber reinforcements. With 1wt.% addition of MWCNT, both K_{IC} and G_{IC} values increased by 121% and 290%, respectively. Along with

the MWCNT addition, when the epoxy is reinforced with a hybrid fiber system, the K_{IC} and G_{IC} values further increase by 237% and 477%, respectively. The uniform dispersion of nano filler particles is an important parameter that governs the fracture toughness and strength characteristics.

Table 3. Tensile properties of epoxy and multiscale composites.

Specimen	Tensile Strength (MPa)	Young's Modulus (GPa)	Elongation at Break (%)
E	36 ± 0.6	1.73 ± 0.01	6.9 ± 0.9
E-C1	61 ± 0.1	2.56 ± 0.02	10.2 ± 0.1
E-C0S2	69 ± 0.8	2.88 ± 0.03	10.2 ± 0.2
E-C1S2	83 ± 2.0	3.18 ± 0.80	10.5 ± 0.6
E-C0S2B2	72 ± 1.8	2.96 ± 0.80	10.7 ± 0.8
E-C1S2B2	99 ± 2.1	3.44 ± 0.90	11.3 ± 0.9

Table 4. Fracture toughness properties of epoxy, nano, and multiscale composite laminates.

Specimen	K_{IC} (MPa·m ^{1/2})	G_{IC} (kJ/m ²)
E	1.9 ± 0.3	1.7 ± 0.4
EC1	4.2 ± 0.2	6.6 ± 0.2
EC0S2	3.5 ± 0.1	4.1 ± 0.5
EC0S2B2	5.3 ± 0.6	7.4 ± 0.3
EC1S2	4.5 ± 0.8	5.1 ± 0.7
EC1S2B2	6.4 ± 0.8	9.8 ± 0.5

Flexural Properties

The flexural tests on epoxy composites were carried out in a three-point bending mode. Figure 4 reveals that the addition of MWCNTs helps in increasing the flexural strength of the composites. In fact, the epoxy resin exhibited a flexural strength of 100 MPa, while it has been seen that E-C1 with 1wt.% of MWCNT improves the flexural strength by 35%. Epoxy composites reinforced with two layers of sisal and basalt fiber layers each exhibited an increase in flexural strength by 120%. The sample with 1 wt.% of MWCNT and hybrid fiber reinforcements revealed the maximum improvement in flexural strength, which augments the confinement effect of FRP wrapping on concrete. The available free volume is reduced significantly upon close packing of polymer chains and attractive polar forces, which, along with the Van der-Waals bonding, are generated between the polymer chains upon MWCNTs incorporation [51]. Thus, the epoxy chains are capable of bearing extra loads.

3.2. Effect of FRP Confinement on Concrete—Group B Specimens

The specimens in Group B were considered to study the influence of the newly developed confining system on the performance of cylinders under uniaxial cyclic loading. Epoxy-based composites reinforced with MWCNTs were applied in between fiber layers as adhesive.

3.2.1. Axial Compressive Behavior

To analyze the influence of cyclic loading on different confinement systems, three sets of specimens were considered: unconfined specimens, epoxy-based FRP confined specimens, and epoxy-based FRP filled with MWCNT confined specimens. The test consists of repeated axial compression with decompression and recompression cycles, and at the end of each cycle, the strain in the next cycle is incremented by 1%. The load values per cycle and the corresponding displacements can be directly recorded from the system.

Table 5 reports the compressive test results exhibited by different confining systems under uniaxial cyclic loading. The ultimate axial strength corresponding to confined specimens includes the ultimate axial strength of both the concrete core and the confined FRP system, which was recorded during the specimen failure. The corresponding axial deflections were also recorded alongside use of a digital data acquisition system.

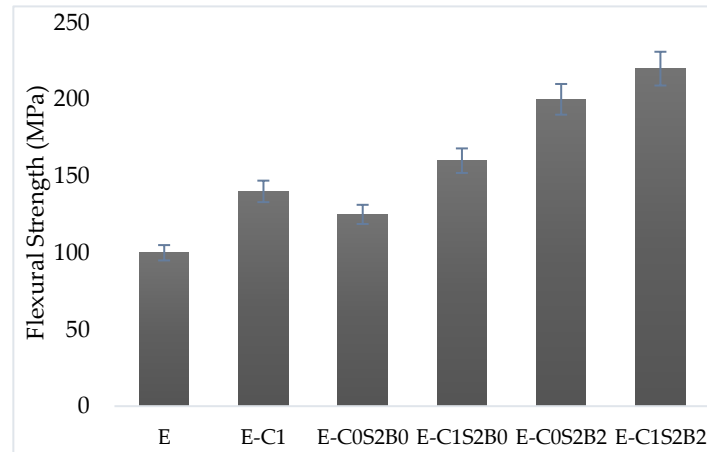


Figure 4. Flexural strength of epoxy, nano and multiscale composites.

Table 5. Axial cyclic compression test results.

Sl No	Specimen	Compressive Strength (MPa) (f'_{cc} or f'_{co})	Strength Enhancement (%)	Confinement Effectiveness f'_{cc}/f'_{co}	Axial Compressive Strain (%)
1	CS	17 ± 0.3	-	-	0.93
2	C-C0S2	28 ± 0.6	52.14	1.521	1.27
3	C-C1S2	29 ± 0.2	55.68	1.557	1.33
4	C-C0S2B2	31 ± 0.3	66.50	1.665	1.54
5	C-C1S2B2	32 ± 0.2	70.51	1.705	1.58

Unconfined Specimens

The unconfined concrete cylinders were considered to be the control specimens (CS). Here the ultimate failure was reached with the development of extreme concrete cracks propagating throughout the column height under axial compression. Since there were no confinements present, these specimens failed due to crushing. The failure was constituted to be sudden cracking along with severe crushing without any prior warning as an indication of catastrophic failure [6,42]. The unconfined cylinders failed to take large loads with development of large longitudinal cracks formed on the periphery of the cylinders as evident from Figure 5. CS specimens experienced severe damage of the concrete core along with multiple cracks on the outer surface, followed by the complete crushing of the concrete core during the 3rd cycle. This was due to the weakening of concrete strength upon exposure to multiple loading cycles. The ultimate failure mode was characterized by shearing and splitting of concrete. The compressive strength exhibited by unconfined specimens under axial cyclic loading is reported in Table 5. The unconfined concrete strength is represented as f'_{co} . The average compressive strength offered by unconfined specimens during axial cyclic loading was noted as 24.36 MPa.

Epoxy-Based FRP Confined Specimens

To analyze the influence of epoxy-based FRP systems as confinement around concrete surfaces, two types of FRP systems were primarily considered. These include two layers of sisal FRP system and four layers of hybrid sisal basalt FRP system. They were effectively

wrapped around the concrete specimens as listed in Table 2 (group B) and considered for the experimental study. The unconfined concrete strength is represented as f'_{cc} . The ultimate failure of epoxy-based FRP confined specimens was basically due to the ultimate failure of both the concrete core and the FRP wraps. When specimens confined with individual sisal FRP sheets (i.e., SFRP) were considered, they failed in a sudden manner with a thunderous sound due to the rupture of external FRP confinement. The failure mechanism exhibited by specimens wrapped with sisal FRP as inner confinement and basalt FRP as external confinement was different from that of individual SFRP-confined specimens. When C-C0S2B2 specimens are considered, the rupture of inner and outer confinements do not occur simultaneously. In these specimens, even before reaching the ultimate loading stage, the inner FRP sheets (i.e., SFRP) ruptured completely and loudly, even if the damage was not visible from the exterior. When the ultimate loading stage is approached, the outer FRP layers (i.e., BFRP) ruptured gradually around the top and bottom ends of the specimens. In both SFRP- and HSBFRP-confined specimens, the ultimate failure pattern was marked as the single line continuous cracking of the FRP laminate as observed from Figure 6. The rupture started from the top end and progressed to the bottom end, without formation of any other alternative cracks. Similar results were stated in earlier studies on sisal and jute FRP confinement [52]. The ultimate stress capacity exhibited by epoxy-based FRP-confined specimens along with axial strain under cyclic axial loading are given in Table 5.



Figure 5. Failure patterns of unconfined specimens.

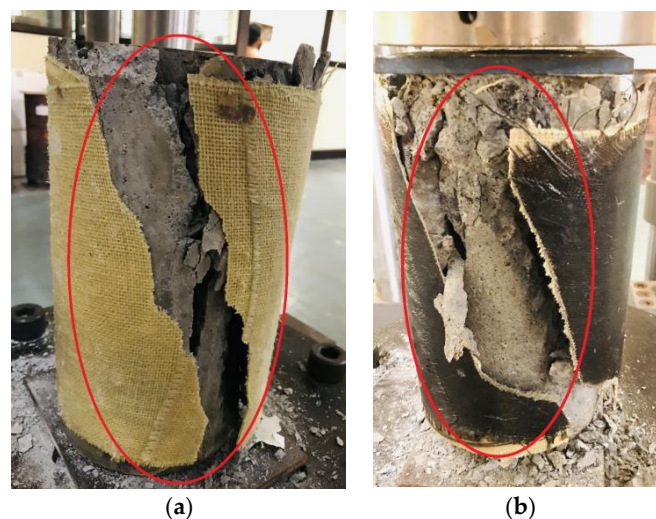


Figure 6. Failure pattern of (a) C-C0S2 (b) C-C0S2B2.

The SFRP confined specimens recorded an increase in axial load carrying capacity by 53%, while the HSBFRP-confined specimens exhibited an increase in strength of 67% when compared with unconfined ones. In both types of FRP composites, even though there were ruptures of FRP layers, a clear debonding of FRP wraps from the concrete surface was not observed. This can be considered evidence of proper bonding between the concrete core and FRP confinement as reported in similar studies [17,20]. The concrete burst after the FRP fracture was more prominent in SFRP-confined specimens compared to HSBFRP-confined specimens. The HSBFRP-wrapped specimens displayed higher ultimate load carrying capacity, and these specimens even after exhibiting signs of failure underwent further axial deflections before ultimate failure. During the ultimate failure condition of HSBFRP confined cylinders, the ultimate load carrying capacity of both the FRPs were exploited. It was therefore inferred that the HSBFRP confinement not only increased the ultimate load carrying capacity but also enhanced the axial deformations.

MWCNT Incorporated Epoxy-Based FRP Confined Specimens

The influence of the incorporation of 1wt.% of MWCNT in the epoxy matrix of the FRP was also considered in this study. During the cyclic loading, characteristic sounds could be heard as an indication of the formation of micro cracks within the concrete core and the confined FRP jackets, serving as early warning before failure. On reaching the ultimate load, both the FRP confinement systems failed with an explosive sound. The composite wrapping layers failed gradually. As evident from Table 5, there was a considerable enhancement in the axial load carrying capacity for C-C1S2 and C-C1S2B2 specimens relative to C-C0S2 and C-C0S2B2. The enhanced axial strength and strain of both the FRP confinements could be attributed to the improved load bearing capacity induced by the MWCNTs dispersed in the matrix. Epoxy being the low modulus element within the FRP, it starts cracking initially during the loading process. With MWCNTs incorporation, a mechanical interlocking between polymer chains and nanotubes is induced. Further, a bridging effect is developed, which enables the transfer of stress between the low modulus matrix material and high modulus MWCNTs. The cracks generated in the concrete core propagated to the FRP layers. The presence of MWCNTs could deflect and bridge the micro cracks as schematically illustrated in Figure 7 [37].

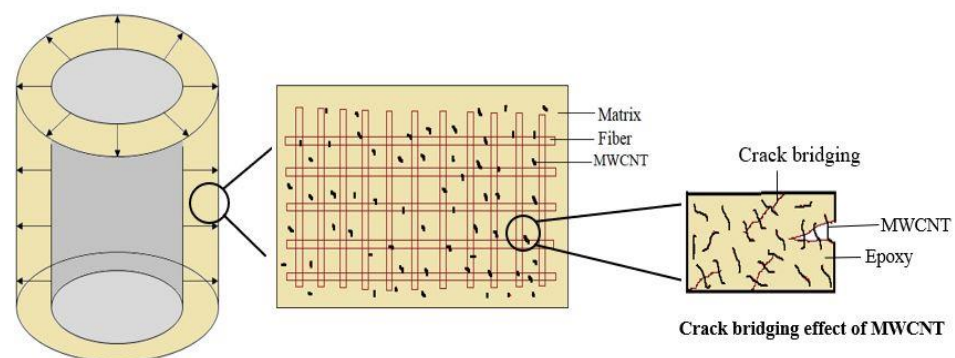


Figure 7. Schematic representation of bridging effect of MWCNT in epoxy.

In the case of neat epoxy FRP-confined specimens there was no evidence of crack formation in the FRP layers during cyclic loading. However, at the final stage, the FRP layers also failed, as seen in Figure 8. The cracks originated from at the top end of the FRP propagated axially in the entire height of the specimen. The bursting of concrete through the cracks marks the failure of specimens, primarily due to FRP rupture [24]. According to the failure modes, the FRP rupture pattern and the cracks in the inner concrete core of the C-C1S2 and C-C1S2B2 are significantly governed by the type of confinement. The splitting failure of the FRP wraps was limited by the superior lateral confinement offered by HSBFRP-confined specimens with MWCNTs, while it was more pronounced when SFRP-

confined specimens were considered [18]. When C-C1S2B2 specimens are considered, even while undergoing higher axial strains, the core is seen to be widely cracked, and still, it continues taking axial load due to the bonded fiber layers. During every unloading cycle, the FRP wraps redistribute the hoop stress around the concrete core. The C-C1S2 specimens suffered severe damage to the concrete core followed by fracture of the composite layers during the 4th cycle at a strain of around 1.55%. On the other hand, the HSBFRP- confined specimen with incorporated MWCNTs C-C1S2B2 failed during the 5th cycle, reaching stresses at 32.05 MPa at a strain around 1.705%. Hence the hybrid-confinement in columns with the addition of MWCNT enhanced the load carrying and deformational capacity of the concrete core.

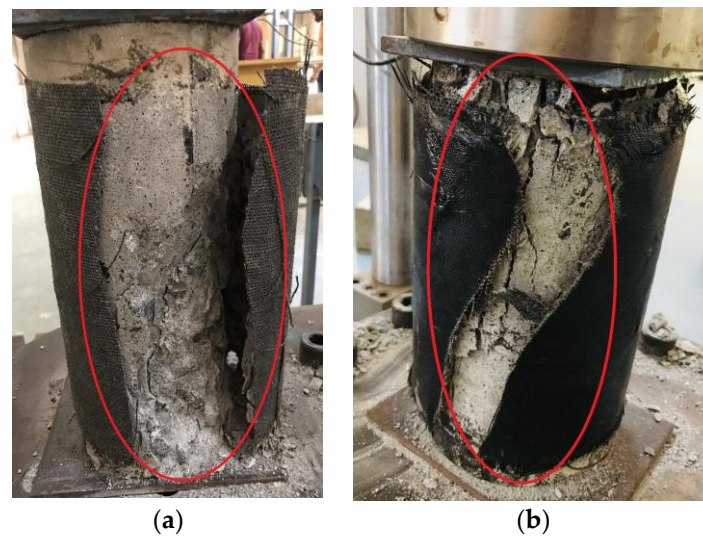


Figure 8. Failure pattern of (a) C-C1S2 (b) C-C1S2B2.

3.3. Efficiency of Wrapping in Concrete Columns

The enhanced axial load carrying capacity observed in cylinders is primarily due to the confining pressure contributed by the FRP layers surrounding the concrete core. The confinement effectiveness is represented as the ratio of the compressive strength of the confined specimens to that of the unconfined ones (f'_{cc}/f'_{co}) [10]. It was evident that the HSBFRP system manifested improved performance due to the combined effect of sisal and basalt FRP systems. When hybrid confinements are considered, the nano filler modified category (C-C1S2B2) recorded the maximum enhancement in axial load carrying capacity of the unconfined concrete core. The sisal-based FRP confinement was also capable of improving the load carrying capacity of the concrete core under cyclic axial compressive loading. The enhanced confinement effectiveness for C-C0S2, C-C1S2, C-C0S2B2, and C-C1S2B2 are 1.521, 1.557, 1.665, and 1.705, respectively, compared to unconfined specimens. Irrespective of the type of FRP confinement, the effect of MWCNT in developing confining pressure to resist the hoop stresses during axial compression was vivid. This could be evidenced from the enhancement in the axial load carrying capacity by 56–71% upon MWCNT modification of epoxy. When the maximum hoop stress is exerted by the concrete core during axial compression, the FRP layers reach its ultimate strain value, and the confinement fails due to the rupture of FRP. The ultimate tensile strain offered by FRP was influenced by the number of FRP wraps. The four-layered MWCNT incorporated HSBFRP offered an improved confining effect compared to two-layered SFRP confinements.

3.4. Stress–Strain Behavior

The mechanical behavior exhibited by FRP confined specimens under axial cyclic loading was assessed in terms of their stress–strain response. Figure 9 presents the stress–strain response of unconfined plain concrete specimens during cyclic loading. The unconfined

specimens reached the peak stress of 17.36 MPa at a strain of 0.93%. The unconfined specimens undergo a sudden brittle failure during the third cycle. The stress–strain curves corresponding to FRP confined concrete specimens are displayed in Figures 10–13. It is worth mentioning that the FRP confined columns exhibited a ductile behavior. The initial regions of the stress–strain curve till the third cycle exhibited a similar trend to that of the unconfined specimens. During this period, since the deformation of concrete is negligible, the effect of FRP confinement is not fully activated. Eventually, the confinement effect is activated during the subsequent cycles on reaching their ultimate compressive strength. The ultimate stress was 28.6 MPa at 1.27% strain for SFRP confined specimens during the fourth cycle. The same SFRP confinement when incorporated with MWCNT could record 29.2 MPa at a strain of 1.33% during the fourth cycle. A drop in the stress values could be observed during the fifth cycle, obviously due to the fracture of FRP layers.

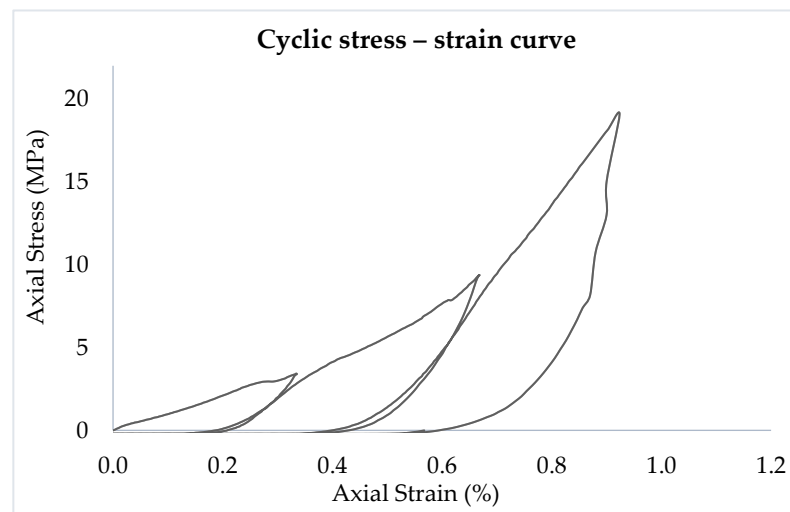


Figure 9. Axial stress versus axial strain curves of CS concrete cylinder under cyclic axial load.

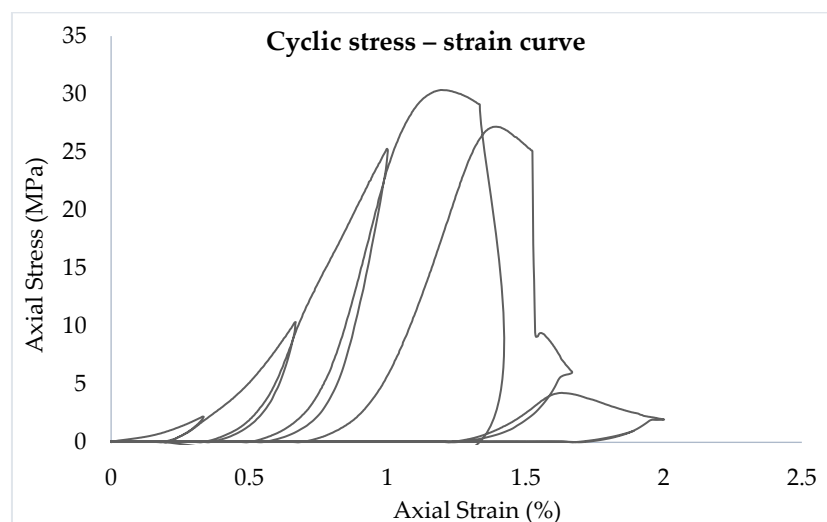


Figure 10. Axial stress versus axial strain curves of C-C0S2 concrete cylinder confined with epoxy-based SFRP under cyclic axial load.

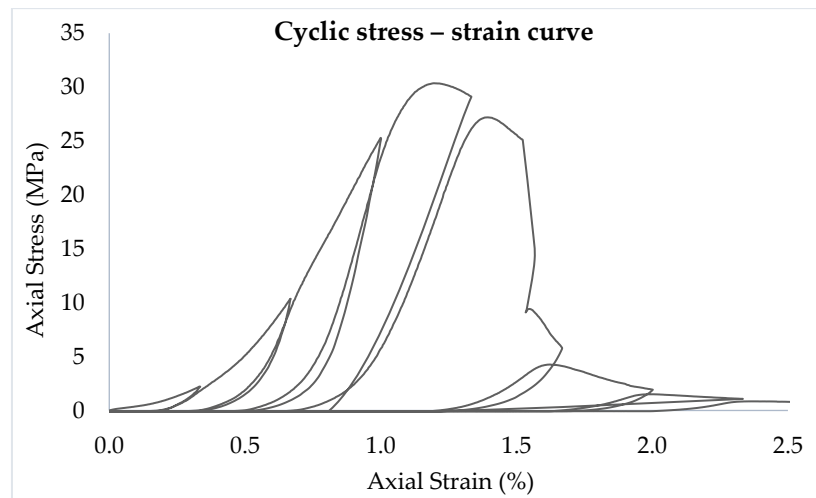


Figure 11. Axial stress versus axial strain curves of C-C1S2 concrete cylinder confined with MWCNT incorporated epoxy-based SFRP under cyclic axial load.

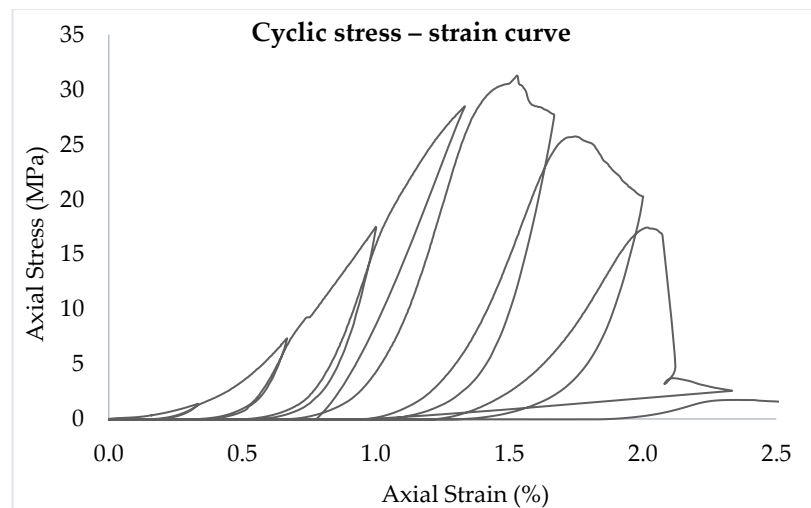


Figure 12. Axial stress versus axial strain curves of C-C0S2B2 concrete cylinder confined with epoxy-based HSBFRP under cyclic axial load.

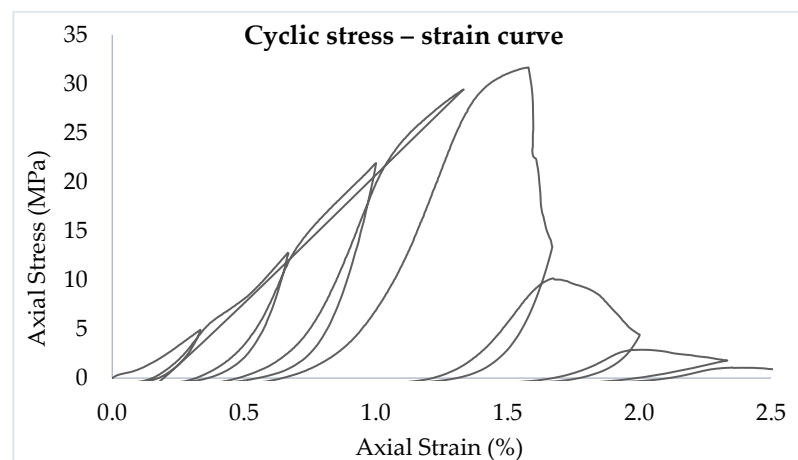


Figure 13. Axial stress versus axial strain curves of C-C1S2B2 concrete cylinder confined with MWCNT incorporated epoxy-based HSBFRP under cyclic axial load.

The specimens C-C0S2B2 and C-C1S2B2 were investigated to study the effect of the HSBFRP confinement. As shown in Figures 12 and 13, the specimens presented a similar stress–strain behavior. During the fifth loading cycle, the ultimate stress capacity exhibited by C-C0S2B2 was 28.49 MPa at 1.54% strain, while C-C1S2B2 exhibited an ultimate stress capacity of 31.58 MPa at 1.58% strain. The specimen C-C1S2B2 exhibited an improved load-bearing response. From the stress–strain results, it is evident that the MWCNT-modified FRP strengthening system could restrict the early crushing of the concrete members under axial cyclic loading with appreciable strain. These results suggest that MWCNT incorporated HSBFRP confinement can serve as an efficient confining reinforcement to resist dynamic loads.

3.5. Mathematical Models

Ultimate Strength Models for FRP Confined Specimens

Numerous research studies, including experimental and analytical works, have been carried out to find the compressive strength exhibited by FRP-confined columns when tested under cyclic axial compressive loading. Most of the available strength models were based on empirical investigations, with an aim that the developed models should predict the ultimate strength of the FRP-confined columns. Several models are available to predict the ultimate strength of FRP-confined specimens, and studies have revealed that the models are influenced by the type of confinement [53–56]. Under the action of cyclic axial compression, tensile stress will be developed around the FRP confinement in hoop direction, and for circular column specimens, it is assumed that the lateral confining pressure developed around the column is uniform. Upon loading, the concrete enlarges laterally, and the confining pressure rises, leading to the failure of FRP layers.

The lateral confining pressure developed is calculated as [42],

$$f_1 = \frac{2tf}{D} = \frac{2tE\varepsilon}{D} \tag{1}$$

where the diameter of the concrete cylinder is denoted as D (mm), the thickness of the FRP layers as t (mm), the modulus of elasticity of FRP as E (N/mm^2), and the ultimate tensile strength of FRP as f (N/mm^2). Based on the existing models [54–56] of FRP-confined systems, the equation for confined compressive strength is given as:

$$f'_{cc} = f'_{co} + k_1 \times f_1 \tag{2}$$

where k_1 is the coefficient of confinement effectiveness, which is the ratio of the compressive strength of the confined specimens to that of the unconfined ones, and its value depends on the experimental results and type of confinement.

Figure 14 depicts a relation correlating the lateral confining pressure and ultimate compressive strength exhibited by epoxy-based SFRP, MWCNT incorporated epoxy-based SFRP, epoxy-based HSBFRP, and MWCNT incorporated epoxy-based HSBFRP- confined cylinders, respectively. The straight line has been fitted with a confidence level of 95%. From the Figure, it is noticeable that the confining effect of FRP is in agreement with the confining pressure developed within the FRP and concrete core. The strength model can be expressed as

$$f'_{cc} = 25.047 + 2.9586 f_1 \tag{3}$$

The unconfined concrete strength (f_{co}) is found to be $24.3 \text{ N}/\text{mm}^2$ as per the experimental study which is found to be close to the analytical value of $25.0 \text{ N}/\text{mm}^2$ obtained from Equation (3). On dividing both sides of the Equation (3) with f_{co} the equation is modified as

$$\frac{f_{cc}}{f_{co}} = 1 + 2.9586 \frac{f_1}{f_{co}} \tag{4}$$

The confinement effectiveness is represented as f_{cc}/f_{co} . From the equation, it is evident that the strengthening ratio is inversely proportional to unconfined strength and directly

proportional to the strength of FRP. The comparative study between the experimental and analytical results corresponding to axial stress is presented in Table 6, where the deviation in experimental and analytical results is found to be less than 1%. Thus, the proposed model is in agreement with the experimental study establishing its suitability for the prediction of peak compressive strength of FRP-confined specimens under axial cyclic loading.

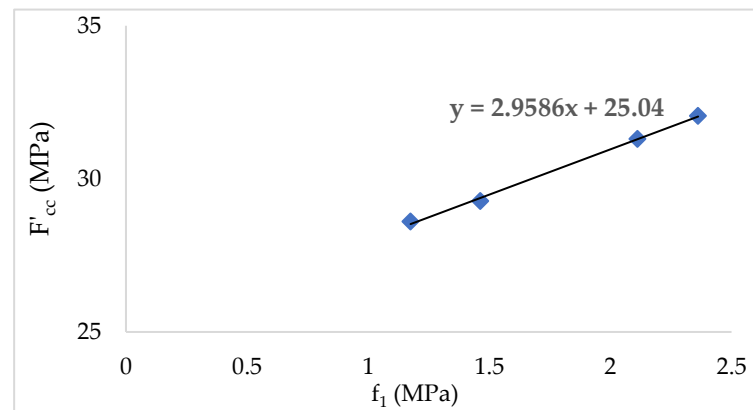


Figure 14. Peak compressive strength vs. lateral confining pressure.

Table 6. Comparison of experimental and analytical confined compressive strength.

Specimen	Confined Compressive Strength f_{cc} (MPa)		Percentage Difference (%)
	Experimental Results	Analytical Results	
C-C0S2	28.6	28.5	0.28
C-C0S2B2	31.3	31.2	0.03
C-C1S2	29.2	29.3	0.36
C-C1S2B2	32.2	32.1	0.31

4. Conclusions and Future Outlook

The present paper presents the experimental investigation of a newly developed epoxy-based hybrid FRP confinement containing MWCNTs to be used as a wrapping layer on concrete columns under compressive loading. In particular, the objective of the study is to assess the suitability of the proposed method in columns subjected to cyclic loading. In both epoxy nano and multiscale composites, the presence of MWCNT and its uniform dispersion contributes to the improved mechanical properties. The presence of 1wt.% of MWCNT raised the flexural strength of nanocomposites by 60% and that of multiscale composites by 120% with respect to neat epoxy. From the experimental data, the following results can be highlighted:

- As evident from the test results under multiple load compression cycles, the load carrying capacity of the structures could be enhanced remarkably with FRP confinements. A noticeable additional improvement could also be accomplished with MWCNT modification of epoxy;
- The enhanced strength and ultimate strain by 60 to 75% of the confined specimens are found to be influenced by the type of FRP confinement and MWCNT modification of the epoxy matrix. Hybrid confinement was more effective than sisal FRP in terms of strength enhancement;
- When hybrid confinement is taken into consideration the outer FRP layers aided in resisting the axial compressive loads post ultimate loading and thereby resisting catastrophic failure in columns;
- MWCNT incorporated epoxy wrapped specimens were capable of giving early warning in the form of small cracking sounds as an indication of the formation of microcracks before ultimate failure;

- An empirical equation is developed to predict the peak compressive strength of FRP-confined concrete. The results of the proposed model and experimental results were found to be in good agreement.

Hence, based on this study, it is evident that MWCNT incorporated epoxy-based hybrid confinement systems is a viable option for structural strengthening and retrofitting. The epoxy modification exhibited better response to cyclic loading, and the newly developed system can be adopted in structures susceptible to seismic damages.

As future work, the confinement approach may be extended to reinforced concrete structures and long columns. Different types of nano fillers and surface treatments for better attachment of nano fillers onto the surface of the fiber for modifying the interface between the matrix and fiber can be explored.

Author Contributions: L.J.: Conceptualization, Methodology, Investigation, Formal Analysis, Validation, Writing—original draft preparation; M.K.M.: Conceptualization, Methodology, Supervision, Formal Analysis, Writing—review and editing; K.J.: Conceptualization, Methodology, Supervision, Formal Analysis, Writing—review and editing; A.P.: Formal Analysis, Writing—review and editing. All authors have read and agreed to the published version of the manuscript.

Funding: This research received no external funding.

Data Availability Statement: Not applicable.

Acknowledgments: The authors are grateful to Center of Excellence in Advanced Materials and Green Technologies (CoE-AMGT), Amrita School of Engineering, Coimbatore, Amrita Vishwa Vidyapeetham, India for TGA analysis.

Conflicts of Interest: The authors declare no conflict of interest.

References

1. Padanattil, A.; Lakshmanan, M.; Jayanarayanan, K.; Mini, K.M. Strengthening of Plain Concrete Cylinders with Natural FRP Composite Systems. *Iran. J. Sci. Technol. Trans. Civ. Eng.* **2019**, *43*, 381–389. [[CrossRef](#)]
2. Tang, Y.; Wang, Y.; Wu, D.; Liu, Z.; Zhang, H.; Zhu, M.; Chen, Z.; Sun, J.; Wang, X. An Experimental Investigation and Machine Learning-Based Prediction for Seismic Performance of Steel Tubular Column Filled with Recycled Aggregate Concrete. *Rev. Adv. Mater. Sci.* **2022**, *61*, 849–872. [[CrossRef](#)]
3. Rousakis, T.C.; Karabinis, A.I.; Kioussis, P.D. FRP-Confined Concrete Members: Axial Compression Experiments and Plasticity Modelling. *Eng. Struct.* **2007**, *29*, 1343–1353. [[CrossRef](#)]
4. Lam, L.; Teng, J.G. Stress–Strain Model for FRP-Confined Concrete under Cyclic Axial Compression. *Eng. Struct.* **2009**, *31*, 308–321. [[CrossRef](#)]
5. Lam, L.; Teng, J.G.; Cheung, C.H.; Xiao, Y. FRP-Confined Concrete under Axial Cyclic Compression. *Cem. Concr. Compos.* **2006**, *28*, 949–958. [[CrossRef](#)]
6. Pimanmas, A.; Hussain, Q.; Panyasirikhunawut, A.; Rattanapitikon, W. Axial Strength and Deformability of Concrete Confined with Natural Fibre Reinforced Polymers (NFRP). *Mag. Concr. Res.* **2017**, *71*, 55–70. [[CrossRef](#)]
7. Li, P.; Wu, Y.-F. Stress–Strain Behavior of Actively and Passively Confined Concrete under Cyclic Axial Load. *Compos. Struct.* **2016**, *149*, 369–384. [[CrossRef](#)]
8. Zeng, J.-J.; Ye, Y.-Y.; Guo, Y.-C.; Lv, J.-F.; Ouyang, Y.; Jiang, C. PET FRP-Concrete-High Strength Steel Hybrid Solid Columns with Strain-Hardening and Ductile Performance: Cyclic Axial Compressive Behavior. *Compos. Part B Eng.* **2020**, *190*, 107903. [[CrossRef](#)]
9. Taghia, P.; Bakar, S.A. Mechanical behaviour of confined reinforced concrete-CFRP short column-based on finite element analysis. *World Appl. Sci. J.* **2013**, *24*, 960–970.
10. Wu, H.-L.; Wang, Y.-F.; Yu, L.; Li, X.-R. Experimental and Computational Studies on High-Strength Concrete Circular Columns Confined by Aramid Fiber-Reinforced Polymer Sheets. *J. Compos. Constr.* **2009**, *13*, 125–134. [[CrossRef](#)]
11. Tang, Y.; Fang, S.; Chen, J.; Ma, L.; Li, L.; Wu, X. Axial Compression Behavior of Recycled-Aggregate-Concrete-Filled GFRP-Steel Composite Tube Columns. *Eng. Struct.* **2020**, *216*, 110676. [[CrossRef](#)]
12. Ozkılıç, Y.O.; Gemi, L.; Madenci, E.; Aksoylu, C.; Kalkan, İ. Effect of the GFRP Wrapping on the Shear and Bending Behavior of RC Beams with GFRP Encasement. *Steel Compos. Struct.* **2022**, *45*, 193–204. [[CrossRef](#)]
13. Madenci, E.; Özkılıç, Y.O.; Aksoylu, C.; Safonov, A. The Effects of Eccentric Web Openings on the Compressive Performance of Pultruded GFRP Boxes Wrapped with GFRP and CFRP Sheets. *Polymers* **2022**, *14*, 4567. [[CrossRef](#)] [[PubMed](#)]
14. Choi, D.; Vachirapanyakun, S.; Kim, S.-Y.; Ha, S.-S. Ductile Fiber Wrapping for Seismic Retrofit of Reinforced Concrete Columns. *J. Asian Concr. Fed.* **2015**, *1*, 37–46. [[CrossRef](#)]

15. Padanattil, A.; Karingamma, J.; Mini, K.M. Novel Hybrid Composites Based on Glass and Sisal Fiber for Retrofitting of Reinforced Concrete Structures. *Constr. Build. Mater.* **2017**, *133*, 146–153. [[CrossRef](#)]
16. Joseph, L.; Sarath Kumar, P.; Jayanarayanan, K.; Mini, K.M. Strengthening of Plain Concrete Cylinders with Hybrid Composites Based on Basalt and Sisal Fiber Systems. *Mater. Today Proc.* **2022**, *66*, 2444–2448. [[CrossRef](#)]
17. Wahab, N.; Srinophakun, P.; Hussain, Q.; Chaimahawan, P. Performance of Concrete Confined with a Jute–Polyester Hybrid Fiber Reinforced Polymer Composite: A Novel Strengthening Technique. *Fibers* **2019**, *7*, 72. [[CrossRef](#)]
18. Ramesh, M.; Palanikumar, K.; Reddy, K.H. Mechanical Property Evaluation of Sisal–Jute–Glass Fiber Reinforced Polyester Composites. *Compos. Part B Eng.* **2013**, *48*, 1–9. [[CrossRef](#)]
19. Vijaya Ramnath, B.; Junaid Kokan, S.; Niranjana Raja, R.; Sathyanarayanan, R.; Elanchezian, C.; Rajendra Prasad, A.; Manickavasagam, V.M. Evaluation of Mechanical Properties of Abaca–Jute–Glass Fibre Reinforced Epoxy Composite. *Mater. Des.* **2013**, *51*, 357–366. [[CrossRef](#)]
20. Ispir, M.; Dalgic, K.D.; Ilki, A. Hybrid Confinement of Concrete through Use of Low and High Rupture Strain FRP. *Compos. Part B Eng.* **2018**, *153*, 243–255. [[CrossRef](#)]
21. Bouchelaghem, H.; Bezazi, A.; Scarpa, F. Compressive Behaviour of Concrete Cylindrical FRP-Confined Columns Subjected to a New Sequential Loading Technique. *Compos. Part B Eng.* **2011**, *42*, 1987–1993. [[CrossRef](#)]
22. De Luca, A.; Nardone, F.; Matta, F.; Nanni, A.; Lignola, G.P.; Prota, A. Structural Evaluation of Full-Scale FRP-Confined Reinforced Concrete Columns. *J. Compos. Constr.* **2011**, *15*, 112–123. [[CrossRef](#)]
23. Takeuti, A.R.; de Hanai, J.B.; Mirmiran, A. Preloaded RC Columns Strengthened with High-Strength Concrete Jackets under Uniaxial Compression. *Mater. Struct.* **2008**, *41*, 1251–1262. [[CrossRef](#)]
24. Rousakis, T.C.; Karabinis, A.I. Adequately FRP Confined Reinforced Concrete Columns under Axial Compressive Monotonic or Cyclic Loading. *Mater. Struct.* **2012**, *45*, 957–975. [[CrossRef](#)]
25. Cao, Y.-G.; Hou, C.; Liu, M.-Y.; Jiang, C. Effects of Predamage and Load Cyclic on Compression Behavior of Fiber Reinforced Polymer-Confined Concrete. *Struct. Concr.* **2021**, *22*, 1784–1799. [[CrossRef](#)]
26. Salleh, S.Z.; Ahmad, M.Z.; Ismail, H. Properties of Natural Rubber/Recycled Chloroprene Rubber Blend: Effects of Blend Ratio and Matrix. *Procedia Chem.* **2016**, *19*, 346–350. [[CrossRef](#)]
27. Zhou, P.; Li, C.; Bai, Y.; Dong, S.; Xian, G.; Vedernikov, A.; Akhatov, I.; Safonov, A.; Yue, Q. Durability Study on the Interlaminar Shear Behavior of Glass-Fibre Reinforced Polypropylene (GFRPP) Bars for Marine Applications. *Constr. Build. Mater.* **2022**, *349*, 128694. [[CrossRef](#)]
28. Tucci, F.; Vedernikov, A. *Design Criteria for Pultruded Structural Elements*; Elsevier: Amsterdam, The Netherlands, 2021; pp. 51–68.
29. Vedernikov, A.; Safonov, A.; Tucci, F.; Carlone, P.; Akhatov, I. Analysis of Spring-in Deformation in L-shaped Profiles Pultruded at Different Pulling Speeds. *Math. Simul. Exp. Results* **2021**. [[CrossRef](#)]
30. Minchenkov, K.; Vedernikov, A.; Kuzminova, Y.; Gusev, S.; Sulimov, A.; Gulyaev, A.; Kreslavskaya, A.; Prosyany, I.; Xian, G.; Akhatov, I.; et al. Effects of the Quality of Pre-Consolidated Materials on the Mechanical Properties and Morphology of Thermoplastic Pultruded Flat Laminates. *Compos. Commun.* **2022**, *35*, 101281. [[CrossRef](#)]
31. Mittal, G.; Rhee, K.Y.; Mišković-Stanković, V.; Hui, D. Reinforcements in Multi-Scale Polymer Composites: Processing, Properties, and Applications. *Compos. Part B Eng.* **2018**, *138*, 122–139. [[CrossRef](#)]
32. Ervina, J.; Mariatti, M.; Hamdan, S. Effect of Filler Loading on the Tensile Properties of Multi-Walled Carbon Nanotube and Graphene Nanopowder Filled Epoxy Composites. *Procedia Chem.* **2016**, *19*, 897–905. [[CrossRef](#)]
33. Pincheira, G.; Montalba, C.; Gacitua, W.; Montrieux, H.-M.; Lecomte-Beckers, J.; Meléndrez, M.F.; Flores, P. Study of the Effect of Amino-Functionalized Multiwall Carbon Nanotubes on Dry Sliding Wear Resistance Properties of Carbon Fiber Reinforced Thermoset Polymers. *Polym. Bull.* **2016**, *73*, 2287–2301. [[CrossRef](#)]
34. Alhareb, A.O.; Akil, H.M.; Ahmad, Z.A. Impact Strength, Fracture Toughness and Hardness Improvement of PMMA Denture Base through Addition of Nitrile Rubber/Ceramic Fillers. *Saudi J. Dent. Res.* **2017**, *8*, 26–34. [[CrossRef](#)]
35. Mahato, K.K.; Dutta, K.; Chandra Ray, B. Assessment of Mechanical, Thermal and Morphological Behavior of Nano-Al₂O₃ Embedded Glass Fiber/Epoxy Composites at in-Situ Elevated Temperatures. *Compos. Part B Eng.* **2019**, *166*, 688–700. [[CrossRef](#)]
36. Eskizeybek, V.; Ulus, H.; Kaybal, H.B.; Şahin, Ö.S.; Avcı, A. Static and Dynamic Mechanical Responses of CaCO₃ Nanoparticle Modified Epoxy/Carbon Fiber Nanocomposites. *Compos. Part B Eng.* **2018**, *140*, 223–231. [[CrossRef](#)]
37. Sarath Kumar, P.; Jayanarayanan, K.; Deeraj, B.D.S.; Joseph, K.; Balachandran, M. Synergistic Effect of Carbon Fabric and Multiwalled Carbon Nanotubes on the Fracture, Wear and Dynamic Load Response of Epoxy-Based Multiscale Composites. *Polym. Bull.* **2021**, *79*, 5063–5084. [[CrossRef](#)]
38. Sarath Kumar, P.; Jayanarayanan, K.; Balachandran, M. Thermal and Mechanical Behavior of Functionalized MWCNT Reinforced Epoxy Carbon Fabric Composites. *Mater. Today Proc.* **2020**, *24*, 1157–1166. [[CrossRef](#)]
39. Joseph, L.; Kumar, P.S.; Deeraj, B.D.S.; Joseph, K.; Jayanarayanan, K.; Mini, K.M. Modification of Epoxy Binder with Multi Walled Carbon Nanotubes in Hybrid Fiber Systems Used for Retrofitting of Concrete Structures: Evaluation of Strength Characteristics. *Heliyon* **2022**, *8*, e09609. [[CrossRef](#)]
40. Joseph, L.; Madhavan, M.K.; Jayanarayanan, K.; Pegoretti, A. High Temperature Performance of Concrete Confinement by MWCNT Modified Epoxy Based Fiber Reinforced Composites. *Materials* **2022**, *15*, 9051. [[CrossRef](#)]
41. Wu, Y.-F.; Wei, Y. General Stress-Strain Model for Steel- and FRP-Confined Concrete. *J. Compos. Constr.* **2015**, *19*, 04014069. [[CrossRef](#)]

42. Ozbakkaloglu, T.; Lim, J.C. Axial Compressive Behavior of FRP-Confined Concrete: Experimental Test Database and a New Design-Oriented Model. *Compos. Part B Eng.* **2013**, *55*, 607–634. [[CrossRef](#)]
43. Ouarhim, W.; Zari, N.; Bouhfid, R. Mechanical performance of natural fibers-based thermosetting composites. In *Mechanical and Physical Testing of Biocomposites, Fibre-Reinforced Composites and Hybrid Composites*; Woodhead Publishing: Cambridge, UK, 2019; pp. 43–60.
44. Tehrani, M.; Boroujeni, A.Y.; Hartman, T.B.; Haugh, T.P.; Case, S.W.; Al-Haik, M.S. Mechanical Characterization and Impact Damage Assessment of a Woven Carbon Fiber Reinforced Carbon Nanotube–Epoxy Composite. *Compos. Sci. Technol.* **2013**, *75*, 42–48. [[CrossRef](#)]
45. Hossain, M.; Chowdhury, M.; Salam, M.; Jahan, N.; Malone, J.; Hosur, M.; Jeelani, S.; Bolden, N. Enhanced Mechanical Properties of Carbon Fiber/Epoxy Composites by Incorporating XD-Grade Carbon Nanotube. *J. Compos. Mater.* **2015**, *49*, 2251–2263. [[CrossRef](#)]
46. Wang, Y.K.; Xu, Z.W.; Chen, L. Effect of Carbon Nanotubes on Friction and Wear Properties of Glass Fiber/Epoxy Composites. *Appl. Mech. Mater.* **2011**, *44–47*, 2181–2185. [[CrossRef](#)]
47. Mei, H.; Zhang, S.; Chen, H.; Zhou, H.; Zhai, X.; Cheng, L. Interfacial Modification and Enhancement of Toughening Mechanisms in Epoxy Composites with CNTs Grafted on Carbon Fibers. *Compos. Sci. Technol.* **2016**, *134*, 89–95. [[CrossRef](#)]
48. Zhang, J.; Zhuang, R.; Liu, J.; Mäder, E.; Heinrich, G.; Gao, S. Functional Interphases with Multi-Walled Carbon Nanotubes in Glass Fibre/Epoxy Composites. *Carbon* **2010**, *48*, 2273–2281. [[CrossRef](#)]
49. Su, Y.; Zhang, S.; Zhang, X.; Zhao, Z.; Jing, D. Preparation and Properties of Carbon Nanotubes/Carbon Fiber/Poly (Ether Ether Ketone) Multiscale Composites. *Compos. Part A Appl. Sci. Manuf.* **2018**, *108*, 89–98. [[CrossRef](#)]
50. Kim, K.W.; Kim, D.K.; Kim, B.S.; An, K.H.; Park, S.J.; Rhee, K.Y.; Kim, B.J. Cure behaviors and mechanical properties of carbon fiber-reinforced nylon6/epoxy blended matrix composites. *Compos. Part B Eng.* **2017**, *112*, 15–21. [[CrossRef](#)]
51. Kim, M.T.; Rhee, K.Y.; Lee, J.H.; Hui, D.; Lau, A.K.T. Property Enhancement of a Carbon Fiber/Epoxy Composite by Using Carbon Nanotubes. *Compos. Part B Eng.* **2011**, *42*, 1257–1261. [[CrossRef](#)]
52. Sen, T.; Paul, A. Confining Concrete with Sisal and Jute FRP as Alternatives for CFRP and GFRP. *Int. J. Sustain. Built Environ.* **2015**, *4*, 248–264. [[CrossRef](#)]
53. Turgay, T.; Köksal, H.O.; Polat, Z.; Karakoç, C. Stress–strain model for concrete confined with CFRP jackets. *Mater. Des.* **2009**, *30*, 3243–3251. [[CrossRef](#)]
54. Dai, J.-G.; Bai, Y.-L.; Teng, J.G. Behavior and Modeling of Concrete Confined with FRP Composites of Large Deformability. *J. Compos. Constr.* **2011**, *15*, 963–973. [[CrossRef](#)]
55. Chaallal, O.; Shahawy, M.; Hassan, M. Performance of Axially Loaded Short Rectangular Columns Strengthened with Carbon Fiber-Reinforced Polymer Wrapping. *J. Compos. Constr.* **2003**, *7*, 200–208. [[CrossRef](#)]
56. Lam, L.; Teng, J.G. Design-Oriented Stress–Strain Model for FRP-Confined Concrete. *Constr. Build. Mater.* **2003**, *17*, 471–489. [[CrossRef](#)]

Disclaimer/Publisher’s Note: The statements, opinions and data contained in all publications are solely those of the individual author(s) and contributor(s) and not of MDPI and/or the editor(s). MDPI and/or the editor(s) disclaim responsibility for any injury to people or property resulting from any ideas, methods, instructions or products referred to in the content.